Effect of grid size and initial conditions on vortex-induced vibration of a circular cylinder

by Nurhasni Hasan

Submission date: 09-Aug-2024 01:06AM (UTC-0500)
Submission ID: 2429404283
File name: onditions_on_vortex-induced_vibration_of_a_circular_cylinder.pdf (4.41M)
Word count: 10293
Character count: 52018

Ocean Engineering 263 (2022) 112332

Contents lists available at ScienceDirect

Ocean Engineering

journal homepage: www.elsevier.com/locate/oceaneng

Effect of grid size and initial conditions on vortex-induced vibration of a circular cylinder

Syed Ahmad Raza [a,b], Yosua Heru Irawan [a], Ming-Jyh Chern [a,*]

[a] Department of Mechanical Engineering, National Taiwan University of Science and Technology, Taipei 106335, Taiwan
[b] Department of Mechanical Engineering, NED University of Engineering & Technology, Karachi 124087, Pakistan

ARTICLE INFO

Keywords:
Direct-forcing immersed boundary method
Synchronization
Lock-in region
Grid refinement
Smagorinsky model

ABSTRACT

A direct-forcing immersed boundary (DFIB) method was used with an in-house parallelized C++ code to simulate vortex-induced vibration (VIV) of a one-degree-of-freedom (1-DOF) elastically mounted circular cylinder in the laminar and turbulent flow regimes. The continuity and Navier–Stokes equations were solved numerically together with the equation of motion to study the VIV response of the cylinder in 3-D. The results were analysed and compared with published literature. The importance of conducting a grid independence study at multiple points inside the lock-in (synchronization) region for VIV simulations has been ascertained through detailed comparisons of coarser and finer grids in each of the flow regimes. In addition, for laminar flows, the effect of the grid on the evolution of the vibration response in the lock-in region was discussed. For turbulent flows, the effect of different initial conditions on VIV amplitude was studied, and a hysteresis phenomenon was observed in the initial and upper branches of the lock-in region. The need for multiple calculation methods of vibration amplitudes in turbulent flows was highlighted.

1. Introduction

Flows over a circular cylinder have been widely studied using experimental and numerical studies. Despite the simple geometry, the generation of vortices in the wake of the cylinder leads to unbalanced forces acting on the cylinder. When allowed to move freely, such forces cause vortex-induced vibrations (VIV) of the cylinder. When the frequency of vortices roughly matches one of the natural frequencies of the system, the cylinder enters into the classical synchronization or "lock-in" mode, which is characterized by large-amplitude oscillations. Cylinders submerged in fluids are important to several types of engineering problems, such as submerged structures or industrial chimneys. Recently, this topic has received renewed interest due to the potential of harnessing energy from VIV using bladeless wind turbines and VIVACE converters (Bernitsas et al., 2008). Such designs typically focus on the single degree-of-freedom (DOF) transverse vibrations of the circular cylinder.

One of the earliest studies characterizing the vortex-excited oscillations was conducted by Ferguson and Parkinson (1967) for subcritical Reynolds numbers in the range of 15,000 to 41,000. Khalak and Williamson (1996, 1997, 1999) carried out a series of experiments to establish benchmark results of vortex-induced vibrations of circular cylinders at low mass and damping ($m^* = 2.4$ and $\zeta = 0.0045$) in turbulent flows. They also defined the VIV response near the lock-in (synchronization) region and identified the initial, upper and lower branches. Anagnostopoulos and Bearman (1992) performed experiments on a circular cylinder undergoing VIV in laminar flow at low Reynolds numbers with varying mass-damping parameters $m^*\zeta = 0.281$ - 0.356 for the first time. Several numerical studies of this phenomenon have also been conducted for laminar and turbulent flow regimes.

Dettmer and Perić (2006) modelled the vortex-induced oscillations of a cylinder in laminar flow using a novel, fully-implicit 2-D method for fluid–rigid body interactions. The Reynolds numbers were changed from 90 to 130. They considered three different grid sizes, and all of them displayed variations in the onset of the lock-in region as well the range of Reynolds numbers where the cylinder undergoes the high lock-in oscillations (Dettmer and Perić, 2006, Figure 6). However, they did not discuss the significance of this issue. Yang et al. (2008) used an embedded boundary method to study oscillations in laminar flow for a single cylinder with one and two DOF, as well as multiple cylinders. Chern et al. (2014) used a DFIB method with a volume of solid (VOS) function to model the VIV of a cylinder with $m^* = 149.1$ and $\zeta = 0.0012$. These investigations used the problem of a cylinder(s) in VIV to evaluate the robustness of their numerical methods.

Several numerical investigations have also been conducted for the turbulent flows over a cylinder undergoing VIV. There are two different approaches to this problem found in the literature. Some studies have

* Corresponding author.
E-mail address: mjchern@mail.ntust.edu.tw (M.-J. Chern).

https://doi.org/10.1016/j.oceaneng.2022.112332
Received 4 April 2022; Received in revised form 22 July 2022; Accepted 12 August 2022
Available online 2 September 2022
0029-8018/© 2022 Elsevier Ltd. All rights reserved.

attempted to follow the experiments of Khalak and Williamson (1997) by conducting simulations over a similar range of reduced velocities (U_R^*) while also matching the Reynolds numbers of the experiment. This would require either a gradual refinement of the grid along with increase in Reynolds numbers or that the grid is fixed at the y^+ of the highest Reynolds number used in the study. Guilmineau and Queutey (2004) used this approach in their RANS study of a low mass-damping elastically mounted cylinder with $m^* = 2.4$ and $m^*\zeta = 0.0$. They used three sets of initial conditions to simulate this problem: from rest, increasing velocity and decreasing velocity. The first initial condition modelled a cylinder initially at rest, which later starts to vibrate at a fixed reduced velocity. The second type of initial condition starts with a cylinder at a low reduced velocity, and then its velocity is increased in small steps. The last condition starts with a high velocity, which is then decreased in steps. Although the initial and lower branches were in good agreement with the experimental results of Khalak and Williamson (1997), they were only able to match the amplitude in the upper branch for the increasing velocity condition. Even in that case, the width of the upper branch is much smaller than the experimental results. Since the other initial conditions only exhibit a lower branch, the authors conclude that a hysteresis phenomenon exists.

In contrast, to avoid the need for successive grid refinement or the computational cost of a very fine grid at relatively higher Reynolds numbers, a constant Reynolds number may be used while varying the reduced velocities only, which implies a change in the cylinder mass rather than the upstream flow velocity. Lucor et al. (2005) conducted 3-D DNS studies at Reynolds numbers of 1000, 2000 and 3000, each over a range of reduced velocities with $m^* = 2.0$ and $\zeta = 0.0$. Their results were in agreement with the "three-branch response model" found in earlier experiments (Khalak and Williamson, 1996, 1997, 1999) and also displayed a large amplitude upper branch at all three Reynolds numbers. However, they concluded that the width and magnitude of the upper branch are affected by the Reynolds number. This finding coincides with the assertion of Sarpkaya (2004) that the numerical results based on varying cylinder mass are difficult to reconcile with the experimental results based on varying upstream velocity.

Several researchers have explored different types of hysteresis phenomena related to the VIV of a cylinder. Prasanth et al. (2011) and Prasanth et al. (2006) attempted to study the effect of blockage on the hysteresis of a cylinder undergoing VIV in the laminar flow region. Navrose and Mittal (2013) studied hysteresis for 2-DOF vibrations of a cylinder at $Re = 10^3$.

The methods used to characterize the amplitude of oscillations or other vibration responses, such as lift and drag forces, are also very important. A reliable method for amplitude characterization is necessary for the comparison of flows at different Reynolds numbers and reduced velocities and to draw suitable conclusions about the nature of fluid–solid interactions under different conditions. It would also help compare results of similar flows across various studies conducted using different approaches. Moreover, the possibility of harnessing energy from vortex-induced vibrations raises new questions about the appropriate characterization strategy. For laminar flows over a cylinder undergoing VIV, almost all past studies have used the maximum amplitude of oscillation (A_{max}) to represent the vibration of the cylinder in their results.

By their nature, turbulent flows are highly random phenomena. Many authors investigating turbulent flows have adopted the same characterization method of using the maximum amplitude, but others have opted to find the average of the ($^1/_{10}$)th of the highest amplitudes ($A_{avg(1/10)}$) obtained during vibration. An overview of the past studies of turbulent flows over cylinders undergoing VIV is presented in Table 1. Except for Lucor et al. (2005), all the studies conducted for cylinders in VIV with one DOF characterize the vibration responses using A_{max}. Two DOF investigations are more commonly found to use $A_{avg(1/10)}$ for characterization. Considering the potential of cylinders in VIV for harnessing energy, both of these characterizations are inadequate because they only consider a single oscillation cycle (in the case of A_{max}) or the highest 10% of the vibrations, although using an average of some form is still preferable.

Since cylinders undergoing VIV are sometimes subject to fluctuations, the duration of observations may also have an impact on the results, but many past investigations have not discussed the lengths of their simulations. For their laminar flow investigation, Dettmer and Perić (2006, Figure 7) have shown the complete time histories for some of their cases. They also note that it takes more than 60 s even to trigger the higher amplitude stable oscillations at the onset of the lock-in region. Consequently, the length of the simulation is different over the range of velocities. In turbulent flow studies, Zhao et al. (2014) used 40 cycles of oscillation to find the maximum amplitudes, whereas Pastrana et al. (2018) averaged over 50 cycles of oscillation to determine $A_{avg(1/10)}$. Guilmineau and Queutey (2004, Figures 4 and 5) represent the time histories of several cases lasting for different periods.

There is no consensus in the published literature on the requirements of grid independence for VIV studies. Zhang and Dalton (1996) test different mesh sizes using drag and lift coefficients for flow past a stationary cylinder, the results for which were reported in Sun and Dalton (1996). Al-Jamal and Dalton (2004) analysed different domain sizes using flow past a fixed cylinder. Other researchers have conducted grid independence tests for flow over an oscillating cylinder but only at a single point. Guilmineau and Queutey (2004) conducted a grid independence test for 1-DOF cylinder undergoing VIV at a point in the upper branch of the lock-in region. Similarly, Navrose and Mittal (2013) and Zhao et al. (2014) conducted grid independence tests at reduced velocities in the lower branch of the lock-in region. None of the mesh dependency studies in these investigations was reported for multiple reduced velocities.

In the present study, numerical experiments are conducted in the laminar ($Re = 90$–115) and turbulent flow ($Re = 10^3$) regimes for a cylinder undergoing one DOF VIV in the transverse direction. Separate grid independence tests are conducted in each of the flow regimes at different reduced velocities. The selected mesh is then used to study the variation of amplitudes over a range of reduced velocities encompassing the initial, upper and lower branches through the lock-in region. Later, a finer grid is utilized to observe changes throughout the lock-in region, and the results are compared with published literature. Investigation of the complete lock-in region using two different grids is conducted, each of which was found to be grid independent outside the lock-in region. As per our literature review, this type of study has not been done before. In the laminar flow regime, the patterns of cylinder oscillations for the two different grids at various reduced velocities are discussed. For the turbulent flow regime, a detailed investigation is conducted using three different initial conditions: U_R^* *from rest*, *increasing* U_R^* and *decreasing* U_R^*.

2. Mathematical and numerical models

The present study has been conducted using an in-house code in C++ based on the Finite Volume Method (FVM). The cylinder is modelled using a direct-forcing immersed boundary method as adopted in Chern et al. (2015), which incorporates a virtual force in the solution of Navier–Stokes equations to represent the solid object. Consequently, even an oscillating cylinder can be modelled simply using a Cartesian grid that is generated only once. A subgrid method is utilized to model the solid edges of the cylinder more precisely. This approach has already been tested and described in detail for 3-D spheres in a recent work by the authors (Raza et al., 2020).

The code is developed using the dimensionless continuity and Navier–Stokes equations for an incompressible Newtonian fluid, which can be expressed as follows:

$$\nabla \cdot \mathbf{u} = 0\,, \tag{1}$$

$$\frac{\partial \mathbf{u}}{\partial t^*} + \nabla \cdot (\mathbf{uu}) = -\nabla p + \frac{1}{\mathrm{Re}} \nabla^2 \mathbf{u} + \mathbf{f}^*\,, \tag{2}$$

Table 1
The calculation methods used for characterizing the vibration responses in turbulent flow in past studies.

Study	Cylinder DOF	Type of study	Calculation method
Khalak and Williamson (1996)	1	Experiment	A_{max}
[illegible] and Dalton (1996)	1	2-D LES	A_{max}
Khalak and Williamson (1997)	1	Experiment	A_{max}
Hover et al. (1998)	2	Experiment	$A_{avg(1/10)}$
Khalak and Williamson (1999)	1	Experiment	A_{max}
Govardhan and Williamson (2000)	1	Experiment	A_{max}
Al-Jamal and Dalton (2004)	1	2-D LES	A_{max}
Guilmineau and Queutey (2004)	1	2-D RANS	A_{max}
Lucor et al. (2005)	1	3-D DNS	$A_{avg(1/10)}$
Pan et al. (2007)	1	2-D RANS	A_{max}
[illegible] et al. (2010)	2	Experiment	$A_{avg(1/10)}$
Navrose and Mittal (2013)	2	3-D DNS	A_{max}
Zhao et al. (2014)	1	3-D DNS	A_{max} [a]
Gsell et al. (2016)	2	3-D DNS	$A_{avg(1/10)}$
Pastrana et al. (2018)	2	3-D DNS	$A_{avg(1/10)}$ [b]

[a] A_{max} from 40 cycles of vibration.
[b] $A_{avg(1/10)}$ over 50 cycles of vibration.

where $\mathbf{u}$, t^*, and p are the fluid flow velocity, time and pressure, respectively. Reynolds number (Re) is given by $U_\infty D/\nu$ with U_∞ as the inlet velocity, D is the cylinder diameter and ν is the kinematic viscosity of the fluid. $\mathbf{f}^*$ is used to represent a virtual force accounting for the direct-forcing due to the solid structure.

The QUICK scheme (Leonard, 1979) has been adopted with the third-order Adams–Bashforth method for the temporal terms. The projection method is used to solve the Navier–Stokes equations in steps, with the first intermediate velocity calculated as

$$\mathbf{u}^* = \mathbf{u}^m + \Delta t \left(\frac{1}{\mathrm{Re}} \cdot \nabla^2 \mathbf{u} - \nabla \cdot (\mathbf{u}\mathbf{u}) \right)^m . \tag{3}$$

Substituting the continuity Eq. (1), the pressure Poisson equation can be solved to find the second intermediate velocity, $\mathbf{u}^{**}$,

$$\mathbf{u}^{**} = \mathbf{u}^* - \Delta t \cdot \nabla p^{m+\frac{1}{2}} . \tag{4}$$

The pressure Poisson equation is solved at every time step using a linear solver based on Bi-Conjugate Gradient Stabilized Method (Bi-CGSTAB) method. The second intermediate velocity ($\mathbf{u}^{**}$) and the volume of solid function, η, (calculation of η is described in Raza et al. (2020)) are used to calculate the virtual force ($\mathbf{f}^*$),

$$\mathbf{f}^* = \eta \frac{\mathbf{u}_s^{m+1} - \mathbf{u}^{**}}{\Delta t} , \tag{5}$$

and the final corrected velocity,

$$\mathbf{u}^{m+1} = \eta \mathbf{u}_s^{m+1} + (1-\eta)\mathbf{u}^{**} , \tag{6}$$

where $\mathbf{u}_s^{m+1}$ represents the structure motion velocity, which will be zero when the structure is stationary. The total force that occurs on the rigid body at any time is given by

$$\mathbf{F} = -\iiint_{\Omega_s} \eta \mathbf{f}^* \mathrm{d}V . \tag{7}$$

The cylinder has a single degree of freedom (1-DOF) and is allowed to oscillate in the transverse direction. Rigid-body motion equation for the transverse cylinder displacement is solved using the fourth-order Runge–Kutta method. The motion of the cylinder needs to be analysed to determine the velocity and position of the cylinder at every timestep.

Table 2
Dimensionless variables for rigid-body motion equations. U_∞ is the free stream velocity, D is the diameter of the cylinder, d_y is its displacement in the y-direction (presumably the direction transverse to flow), and L is the axial length extending throughout the computational domain. The structural parameters are mass of the structure, m_s, structural damping, c, structural stiffness, k, and the natural frequency of the structure, f_n. ρ_f is the density of the fluid while F_x and F_y are the total force in the x- and y-directions, respectively, where x is the presumed direction of flow.

Time	t^*	$\frac{tU_\infty}{D}$
Transverse displacement	Y^*	$\frac{d_y}{D}$
Reduced velocity	U_R^*	$\frac{U_\infty}{f_n D}$
Frequency ratio	f^*	$\frac{f}{f_n}$
Structural damping ratio	ζ	$\frac{c}{2\sqrt{m_s k}}$
Mass ratio	m^*	$\frac{m_s}{\frac{1}{4}\pi\rho_f D^2 L}$
Drag force coefficient	C_D	$\frac{F_x}{\frac{1}{2}\rho_f U_\infty^2 (DL)}$
Lift force coefficient	C_L	$\frac{F_y}{\frac{1}{2}\rho_f U_\infty^2 (DL)}$

As discussed in the literature (Chern et al., 2018), with transverse motion in the y-direction, the governing equation is

$$m_s \ddot{Y} + c\dot{Y} + kY = F_y . \tag{8}$$

This equation can be non-dimensionalized as follows:

$$\ddot{Y} + \frac{4\pi\zeta}{U_R^*}\dot{Y} + \left(\frac{2\pi}{U_R^*}\right)^2 Y = \frac{2C_L(t^*)}{\pi m^*} , \tag{9}$$

where $\ddot{Y}$, $\dot{Y}$ and Y are the normalized dimensionless acceleration, velocity and displacement of the structure's centre. The rigid-body motion is represented by a second-derivative equation. In this equation, $\dot{Y}$ is the transverse component of the structure velocity represented by $\mathbf{u}_s^{m+1}$ in Eq. (6). The streamwise and spanwise components of the structure velocity will be zero for the single DOF cylinder. The dimensionless variables used in Eq. (9) are described in Table 2.

This work explores the vortex-induced vibration of a circular cylinder in both laminar and turbulent flow regimes. Sidebottom et al. (2015) conducted a detailed parametric study for turbulent flow past a circular cylinder and tested various cases with and without a wall model (Spalding's law) as well as two subgrid-scale (SGS) LES models. They did not find any conclusive benefit of the wall model and observed only small differences between the Smagorinsky model and the one-equation eddy viscosity model, as well as noting that a y^+ greater than 30 was not accurate enough. Therefore, the turbulent flow cases in the present work use the Smagorinsky model (Smagorinsky, 1963) to model the eddies smaller than the grid. A typical value of Smagorinsky constant $C_s = 0.1$ has been used with no specific wall model and the y^+ for the various grids tested shown in Tables 5–7. This is in agreement with the findings of Sidebottom et al. (2015) as described earlier.

The computational domain of the cylinder and the associated distances are represented in Fig. 1. A non-uniform grid was used for all the cases in this study, as shown in Fig. 2. The cylinder is placed inside a fine grid, whereas a relatively coarser grid is adopted for areas away from the cylinder. It should be noted that the cylinder is slightly offset to the upstream direction within the fine grid region so that the wake immediately behind the cylinder is also modelled more accurately. The relative lengths of the fine and coarse grid regions remain the same throughout this study, but the fine grid sizes are varied, as described in the respective sections on grid independence. The grid is uniform in the z-direction.

Lei et al. (2001) investigated the effects of spanwise length at $\mathrm{Re} = 10^3$ for flow over a cylinder and found that the spanwise length should be equal to or greater than $2D$. Labbé and Wilson (2007) also conducted a similar study for a range of Reynolds numbers between

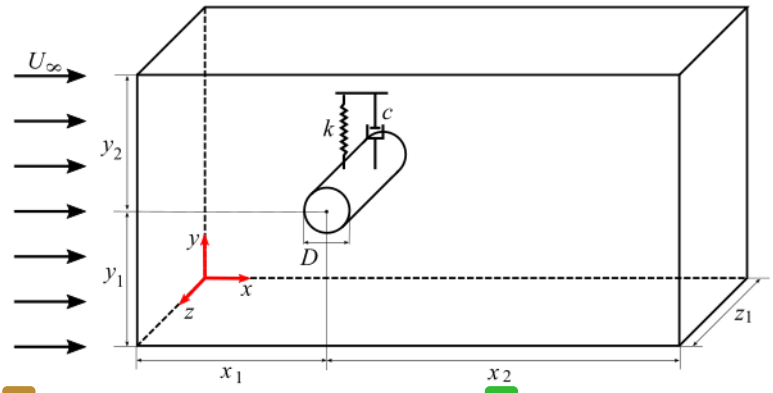

Fig. 1. Computational domain in the present study. The flow occurs in x-direction (streamwise), and the cylinder is allowed to oscillate in the y-direction. The distances for all the cases in this study are: $x_1 = 10D, x_2 = 25D, y_1 = y_2 = 10D$. However, $z_1 = 1D$ for laminar flows and $z_1 = 4D$ for turbulent flows.

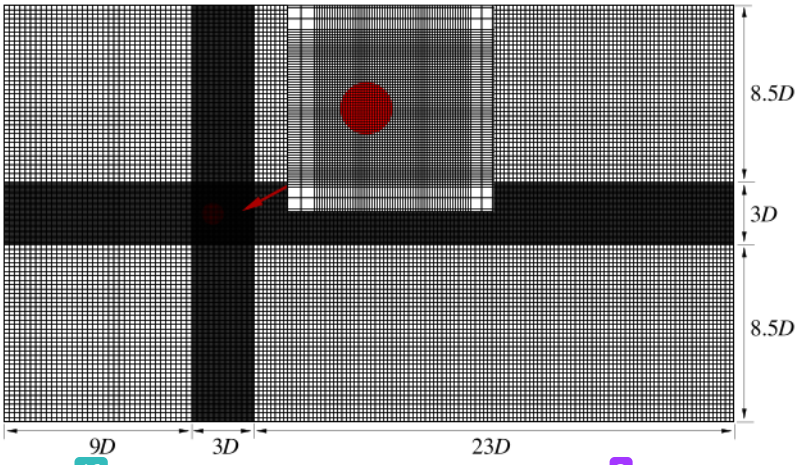

Fig. 2. A side-view of a grid chosen for the present study. A fine grid is selected around the cylinder, and a relatively coarser grid is adopted for areas away from the cylinder. The grid is uniform in the z-direction. The relative lengths of the fine and coarse grid regions remain the same throughout this study, but the fine grid region is adjusted for each case. In this figure, the inset sub-figure shows a closer view of the fine grid distribution around the cylinder.

40 and 10^3. They recommended a spanwise length of four diameters for Reynolds numbers less than 300 and found that a length between $\pi D/2$ and πD was sufficient for higher Reynolds numbers. The laminar flow cases in the present work were conducted in the range of Re = 90–115, where several researchers have found even 2-D studies to be satisfactory (Zhang and Dalton, 1996; Al-Jamal and Dalton, 2004; Guilmineau and Queutey, 2004; Pan et al., 2007). On conducting preliminary tests with longer spanwise lengths, the authors did not find any 3-D fluctuations or any significant effects on the results. Therefore, a $1D$ spanwise length was deemed sufficient for the laminar flow cases. However, to account for the three-dimensional turbulent vortices at Re = 10^3, a longer spanwise length of $4D$ was implemented in the turbulent flow cases.

A constant-velocity boundary condition (Dirichlet) is applied at the inflow with a fixed streamwise velocity and the spanwise and transverse velocity components set to zero. At the outflow boundary, zero-gradient boundary conditions (Neumann) are applied to all the velocity and pressure components. A symmetry boundary condition is used for the lateral boundaries, and a periodic boundary condition is used at the spanwise boundaries. Using a similar DFIB solver, Raza et al. (2021) successfully applied the set of boundary conditions utilized in this work to simulate the physical phenomena of flow through a circular cylinder in a turbulent flow. In order to simulate 3-D VIV simulation, Liu and Jaiman (2018), Pastrana et al. (2018), and Wang et al. (2017) also employed a similar set of boundary conditions.

As discussed, this study was conducted using an in-house solver developed in C++. The solver was parallelized using OpenMP. The solver has been used previously to conduct validations for flows over a stationary sphere, a cylinder as well as a sphere undergoing VIV (Raza et al., 2020, 2021). Most of the simulations for the present work were conducted in a cluster at the Computational Fluid Dynamics Laboratory of the National Taiwan University of Science and Technology (CFDLAB NTUST). It consists of all PowerEdge T630/T640 workstations, with 16, 20 or 32 cores of Intel(R) Xeon(R) (CPU E5-2650 v3 @ 2.30 GHz, CPU E5-2640 v4 @ 2.40 GHz, Silver 4215 CPU @ 2.50 GHz or Gold 6148 CPU @ 2.30 GHz). Some of the simulations were also run on National Center for High-performance Computing (NCHC) Taiwania 1, where the maximum number of cores available on a single machine is 40. Further details of the supercomputer's architecture are available on their website (NCHC, 2021).

3. Results and discussion

The present work investigates laminar flows for Re = 90–115 and turbulent flows at Re = 10^3 over a circular cylinder. The cylinder has

Table 3
Grid independence test for laminar flow at Re = 96 and $U_R^* = 5.345$.

Grid	Grid spacing near the cylinder	$A_{avg(1/10)}$	A_{max}	f^*
Grid A	$\Delta x_s = 0.200; \Delta y_s = 0.200; \Delta z = 0.250$	0.000795	0.000801	0.7867
Grid B	$\Delta x_s = 0.050; \Delta y_s = 0.050; \Delta z = 0.250$	0.008800	0.009300	0.9102
Grid C	$\Delta x_s = 0.015; \Delta y_s = 0.015; \Delta z = 0.250$	0.007400	0.007700	0.9027

Table 4
Grid independence test for laminar flow at Re = 103 and $U_R^* = 5.735$.

Grid	Grid spacing near the cylinder	$A_{avg(1/10)}$	A_{max}	f^*
Grid A	$\Delta x_s = 0.200; \Delta y_s = 0.200; \Delta z = 0.250$	0.0015	0.0015	0.8608
Grid B	$\Delta x_s = 0.050; \Delta y_s = 0.050; \Delta z = 0.250$	0.3430	0.3430	0.9955
Grid C	$\Delta x_s = 0.015; \Delta y_s = 0.015; \Delta z = 0.250$	0.3671	0.3678	0.9955

a single degree of freedom (1-DOF) and is allowed to oscillate in the transverse direction.

In the laminar flow cases, the cylinder was allowed to oscillate from the first timestep and the cases were simulated as long as necessary for the cylinder to achieve stable vibration patterns (refer to Figs. 5, 6, 7 and 8). The larger mass ratio $m^* = 149.1$ with a damping ratio $\zeta = 0.0012$ is used in this investigation. These parameters are similar to the previous VIV study conducted by Chern et al. (2014). Any re-run of the cases always gave the same results.

For the turbulent flow cases, the mass and damping ratios are $m^* = 2.0$ and $\zeta = 0.0$. Here, the zero damping case is used to achieve the larger amplitude (Zhao et al., 2013). In this investigation, the vibration response fluctuated rapidly due to the nature of the flow (refer to Figs. 13 and 14) and needed to be studied over a large number of timesteps. Zhao et al. (2014) simulated each of the results over at least 40 cycles while Pastrana et al. (2018) averaged the results over 50 cycles of cylinder oscillation. During the present investigations in the turbulent flow regime, in each case, the cylinder was initially held stationary for $t^* = (tU_\infty/D) = 250$ and then allowed to oscillate under VIV. For the U_R^* *from rest* initial condition, the simulation was conducted in each case for a total of $t^* = 1500$. Consequently, a larger number of oscillation cycles were recorded for the low U_R^* cases, but for every case, the number of oscillation cycles was more than 100. For the *increasing* U_R^* and *decreasing* U_R^* initial conditions, the cylinder was allowed to oscillate at each U_R^* for $t^* = 250$. Most of the cases, especially in the turbulent flow regime, were repeated three to four times to ensure that the results were consistent.

The two sets of investigations about laminar and turbulent flow regimes are discussed separately in the following sections.

3.1. Grid independence study for laminar regime

The grid independence tests for laminar flow were conducted at reduced velocities of 5.345 (Re = 96) and 5.735 (Re = 103) and the results are presented in Tables 3 and 4, respectively. The grid size of the fine region of the computational grid (as shown in Fig. 2) was refined successively in the x- and y-directions. As shown later in Fig. 3, the first case at $U_R^* = 5.345$ occurs in the initial branch, whereas the second case at $U_R^* = 5.735$ occurs in the lower branch. Separate tests indicated that the refinement of the grid in the coarse regions and the z-direction did not affect the results significantly.

Comparing the different grids in Tables 3 and 4, grid A was found to be inadequate because there is a distinct variation in all of the considered characteristics as the grid is refined from A to B but grids B and C have relatively similar results. Based on the grid independence test and as per conventional practice, grid B could be selected as the optimum grid spacing based on the results so far.

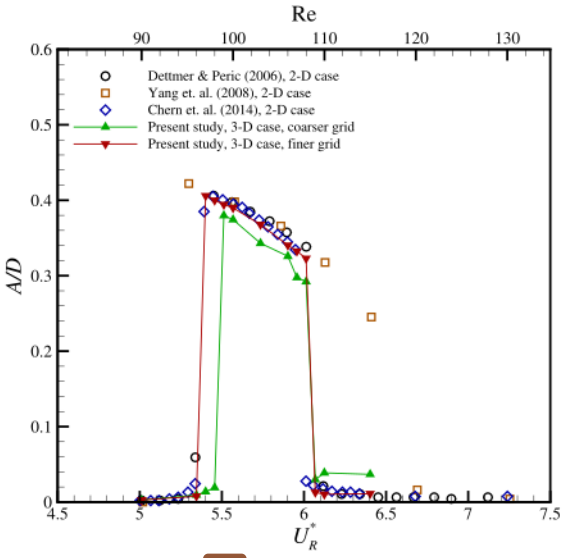

Fig. 3. Maximum amplitudes of the cylinder undergoing VIV in the laminar flow regime at various reduced velocities, compared with published studies.

3.2. Investigation of grid refinement for laminar regime

Despite establishing the grid independence of grid B at two reduced velocities (as shown in Tables 3 and 4), detailed numerical simulations were conducted at several other reduced velocities throughout the synchronization/lock-in region using both grids B (coarser grid) and C (finer grid). The results for maximum amplitude ratio are plotted in Figs. 3. The grid refinement increases the accuracy of upper branch prediction for VIV of the cylinder, especially at the starting and ending reduced velocities of the upper branch. The maximum vibration amplitude throughout the upper branch is very close to the previously published results. The most important observation is that there is a distinct delay in the onset of the lock-in region for the coarse grid. The maximum amplitudes for the coarse grid are also lower than the published results, but after the lock-in region, they are higher than past results. Despite satisfying the grid independence tests for two different reduced velocities, the coarse grid does not represent the lock-in region and VIV phenomenon correctly.

Fig. 4 compares the frequency ratios for the coarse and fine grids with previous results. As in past studies, it is based on the vortex shedding frequency normalized by the structural natural frequency in a vacuum. Both types of grids show good agreement with past results. However, the delay in the onset of the lock-in region for the coarse grid can also be observed from the frequency ratios, which jump to the

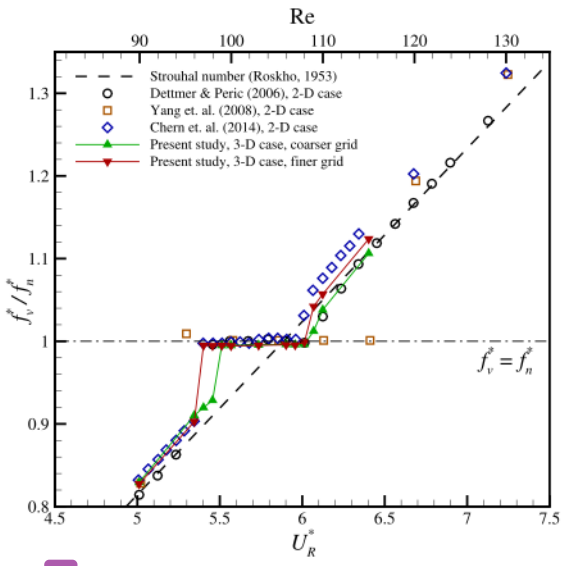

Fig. 4. Vortex shedding frequency ratios for a cylinder undergoing VIV in the laminar flow regime at various reduced velocities, compared with published studies. Roshko (1953, 1954) proposed that the Strouhal number be defined as $St = 0.212(1 - 21.2/Re)$.

$f_v^* = f_n^*$ later than the frequency ratios for the fine grid. Hence, a small lock-in region is observed for the coarser grid.

The time histories of the displacement amplitudes, lift coefficients and drag coefficients at various Reynolds numbers are shown in Figs. 5, 6, 7 and 8. The results show that it is not just the value of the highest amplitude that changes due to grid refinement. The evolution of the ation to a stable response and the time taken for it also changes. For the reduced velocities in the upper branch at Re = 99 and 100, the finer grid achieves a stable vibration much earlier and the ini beating pattern is much shorter (Fig. 5) or nonexistent (Fig. 6). On the other hand, for reduced velocities in the lower branch at Re = 109 and 110, the fine grid takes much longer to evolve into a stable oscillation pattern. For Re = 109, the initial beating phenomenon almost disappears for the coarser grid but exists for a long time in the fine grid. The difference in time histories also indicates that only using the maximum amplitude of displacement, lift coefficients and drag coefficients may not be sufficient to describe these flow phenomena completely.

3.3. Grid independence study for turbulent regime

Extending the analysis from laminar to turbulent flow, a similar investigation was conducted at $Re = 10^3$. A single value of the Reynolds number was chosen to avoid the for grid refinement, which would be necessary for turbulent flows when increasing the Reynol number. Therefore, the effect of the grid size can be analysed over a range of reduced velocities without being affected by the Reynolds numbers. It is suggested th e Smagorinsky constant would also need to be changed for different Reynolds numbers (Al-Jamal and Dalton, 2004), whereas, the prese udy uses a constant value of $C_s = 0.1$. A similar approach was used by Lucor et al. (2005) and Zhao et al. (2014) who also fixed the Reynolds number at $Re = 10^3$.

The grid independence study s carried out at $U_R^* = 2.0$ in the initial branch and $U_R^* = 7.0$ in the lower branch of the -in region. Three types of grids were chosen, with the fine grids in the centre of the computational domain refined in the x– and y–directions progressively. The results are presented in Tables 5 and 6. Since the

Table 5
Grid independence test for turbulent flow at $Re = 10^3$ and $U_R^* = 2.0$.

Grid	Grid spacing near the cylinder	y^+	$A_{avg(1/10)}$
Grid D	$\Delta x_s = 0.15; \Delta y_s = 0.15; \Delta z = 0.2$	15.4	0.0282
Grid E	$\Delta x_s = 0.10; \Delta y_s = 0.10; \Delta z = 0.2$	10.3	0.0510
Grid F	$\Delta x_s = 0.05; \Delta y_s = 0.05; \Delta z = 0.2$	5.1	0.0522

Table 6
Grid independence test for turbulent flow at $Re = 10^3$ and $U_R^* = 7.0$.

Grid	Grid spacing near the cylinder	y^+	$A_{avg(1/10)}$
Grid D	$\Delta x_s = 0.15; \Delta y_s = 0.15; \Delta z = 0.2$	15.4	0.2732
Grid E	$\Delta x_s = 0.10; \Delta y_s = 0.10; \Delta z = 0.2$	10.3	0.6846
Grid F	$\Delta x_s = 0.05; \Delta y_s = 0.05; \Delta z = 0.2$	5.1	0.6761

Table 7
Grid independence test for turbulent flow at $Re = 10^3$ and $U_R^* = 4.0$.

Grid	Grid spacing near the cylinder	y^+	$A_{avg(1/10)}$
Grid D	$\Delta x_s = 0.15; \Delta y_s = 0.15; \Delta z = 0.2$	15.4	0.3560
Grid E	$\Delta x_s = 0.10; \Delta y_s = 0.10; \Delta z = 0.2$	10.3	0.6826
Grid F	$\Delta x_s = 0.05; \Delta y_s = 0.05; \Delta z = 0.2$	5.1	0.7899

cylinder displacement amplitudes for turbul flows do not converge to a stable pattern, unlike the laminar flows, the average of the highest (1/10)th of the amplitudes ($A_{avg(1/10)}$) was calculated and compared for eac se.

It can be seen that for the reduced velocities in both the initial branch as well as the lower branch, there is a significant increase in the average (1/10)th amplitude of the cylinder when the grid is refined from grid D to E. However, further refinement of the grid by decreasing Δx_s and Δy_s from 0.1 in grid E to 0.05 in grid F does not cause any major change in $A_{avg(1/10)}$. Consequently, the results thus far would suggest that grid E is sufficient for this study.

However, based on the conclusions of the l nar flow cases, another grid independence study was carried out in the upper branch of the lock-in region at $U_R^* = 4.0$. From the results given in Table 7, grids E and F lead to significantly different results, unlike for the previous two cases. Therefore, a more detailed analysis of the discrepancy between the two grids for the lock-in region was needed.

3.4. Investigation of grid refinement for turbulent regime

A detailed investigation of the erlying reasons is necessary to see how the grid refinement affects the VIV amplitudes of cylinder. The grids E and F are used to conduct detailed analyses over a range of reduced velocities.

Fig. 9 shows the maximum vibration amplitudes for the two grid sizes, E (coarser grid) and F (finer grid), plotted against previou published studies with similar parameters. The parameters for the experimental study of Khalak and Williamson (1997) are differe om the present study. The experiments were performed in water over a range of Re lds numbers as opposed to a single value of Reynolds number, as in the present case. In order to c pare the reduced velocities and dimensionless natural frequencies with the results of Khalak and Williamson 997), their results have been scaled for comparison as described by Zhao et al. (2014). Pastrana et al. (2018) used a similar conversion for their 2-DOF comparison. Therefore, Figs. 9, 10, 12, 15, 16 and 18 show the scaled results of Khalak and Williamson (1997) for comparison purposes.

It can be deduced from Fig. 9 that the finer grid size exhibits a higher A_{max} for most reduced velocities in the lock-in region. Specifically, at $U_R^* = 4.0$, the resulting amplitudes for the finer grid are even higher than previously published numerical studies and closer to experimental results, whereas, for the coarser grid, the amplitude was much lower.

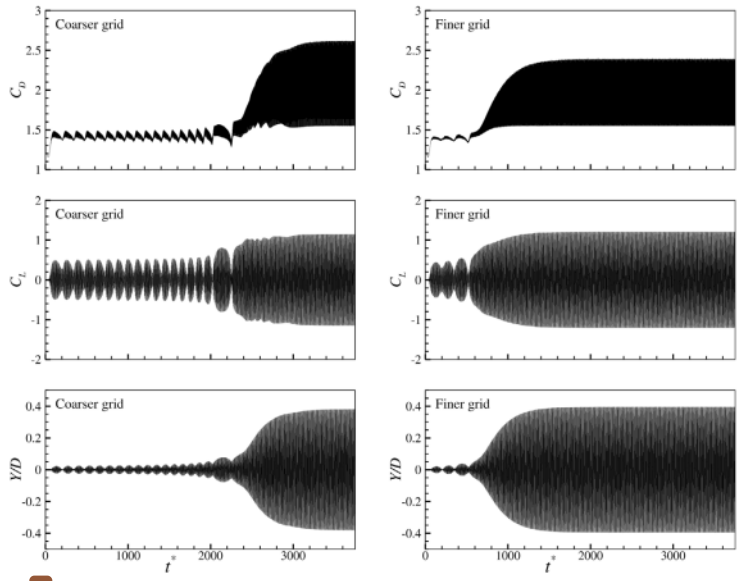

Fig. 5. Time histories of displacement, lift coefficient and drag coefficient at Re = 99 for the coarser and finer grids.

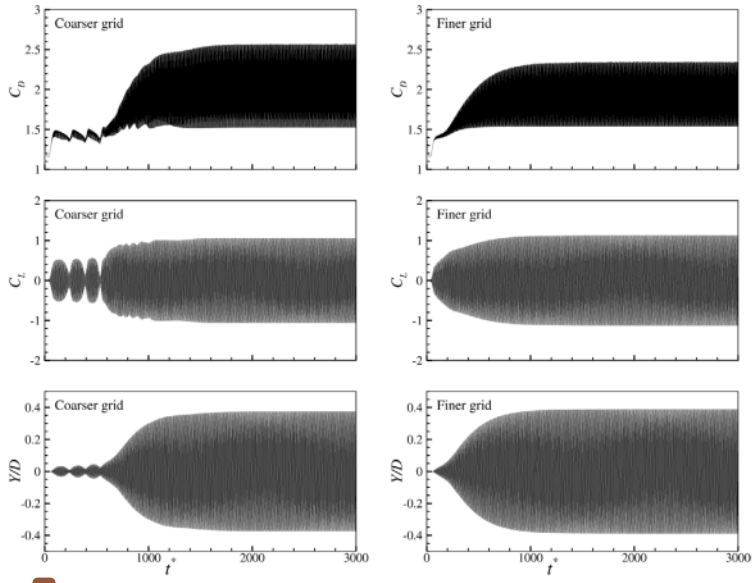

Fig. 6. Time histories of displacement, lift coefficient and drag coefficient at Re = 100 for the coarser and finer grids.

Similar results can be observed for the average of the highest (1/10)th amplitudes ($A_{avg(1/10)}$) in Fig. 10. The trends of A_{max} from Fig. 9 are maintained but the amplitude values are generally lower, which is expected. However, even with $A_{avg(1/10)}$, the result at $U_R^* = 4.0$ for the finer grid is still higher than the previously published numerical results and closer to experimental results, which show A_{max} only. Moreover, although the values of the finer grid amplitudes in the upper branch differ from previous numerical studies, a similar upper branch trend can be observed in Figs. 9 and 10. The initial branch has good agreement with the earlier results, up to the peak value in the upper branch at $U_R^* = 4.0$. However, after that, the present simulations show a sharp decline, which occurs earlier than in other studies leading to a narrower upper branch. This sharp decline is similar to the decline displayed in the numerical results of Guilmineau and Queutey (2004, Figure 3) for the *increasing* U_R^* initial condition, which was conducted for different numerical parameters. However, their upper branch is much more abrupt and narrow and only attains high amplitudes for the *increasing* U_R^* initial condition. The present work can achieve high amplitudes in the upper branch for both the *rest* and *increasing* U_R^* initial conditions, which are discussed later. The amplitudes in the lower branch rise again before falling toward the end of the lock-in region, a trend exhibited by all the past numerical and experimental studies.

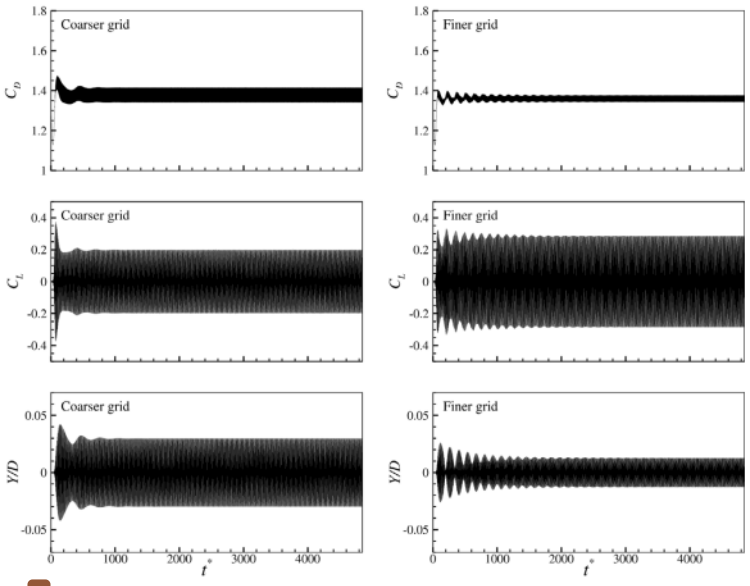

Fig. 7. Time histories of displacement, lift coefficient and drag coefficient at Re = 109 for the coarser and finer grids.

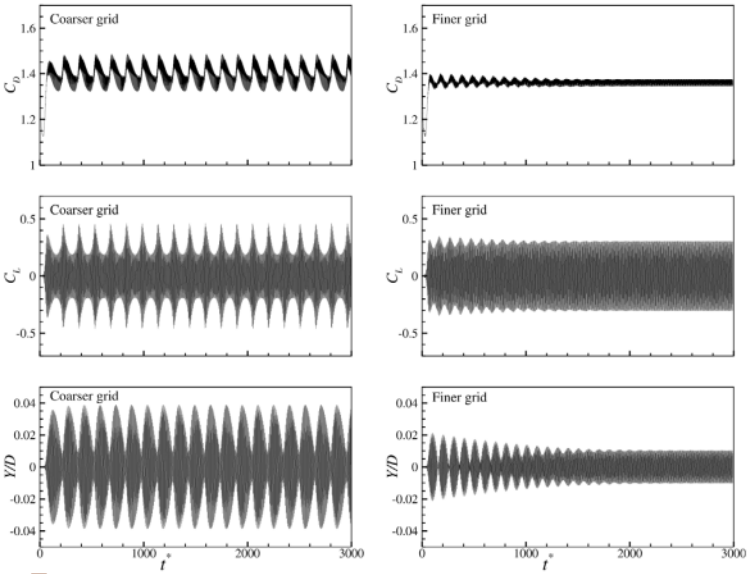

Fig. 8. Time histories of displacement, lift coefficient and drag coefficient at Re = 110 for the coarser and finer grids.

These results suggest that conducting a single grid independence study for a cylinder undergoing VIV may not be sufficient. Even if the grid independence test at $U_R^* = 2.0$ may be dismissed as unimportant because it occurs at the onset of the lock-in region, even the grid independence test at $U_R^* = 7.0$ was not sufficient. Moreover, from Fig. 10, we may conclude that a grid independence test at $U_R^* = 6.0$ or 10.0 would also have led to a similarly misleading result. Therefore, this analysis establishes the importance of conducting multiple grid independence tests inside the lock-in region, preferably near the anticipated maximum amplitudes at the beginning of the upper branch.

As described earlier in Table 1, several previous researchers investigating turbulent flow over a cylinder undergoing VIV have used either A_{max} or $A_{avg(1/10)}$ to characterize the cylinder's vibration. For the present fine grid results, Fig. 11 compares the results of A_{max}, $A_{avg(1/10)}$, $A_{avg(1/3)}$ as well as a simple average of the amplitudes (A_{avg}) of vibration. $A_{avg(1/3)}$ averages the highest one-third amplitudes. Although the trends are the same in the lock-in region, a significant difference is observed between the results in the upper and lower branches of the lock-in region. Unlike laminar flows, the cylinder vibration does not usually evolve into a stable pattern for turbulent flow cases. Therefore, the choice of the type of amplitude presented in the result becomes important, especially when carrying out a comparison between different types of studies, as has been done in the present work. Due to the highly fluctuating nature of turbulent flows, the maximum

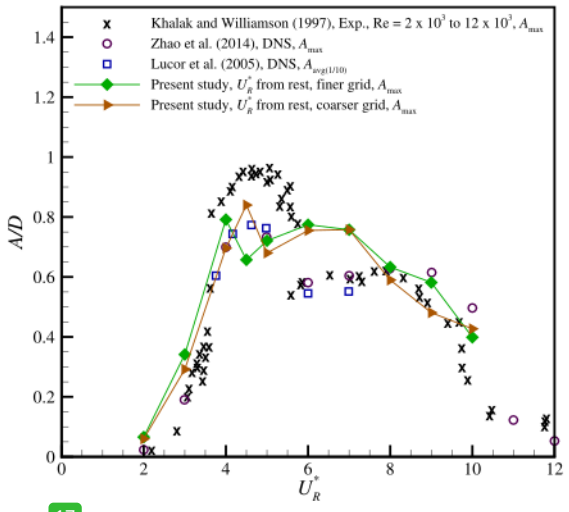

Fig. 9. Maximum vibration amplitudes over a range of reduced velocities at Re = 10^3 with the *rest* initial condition for the coarse and fine grids, compared with previously published studies.

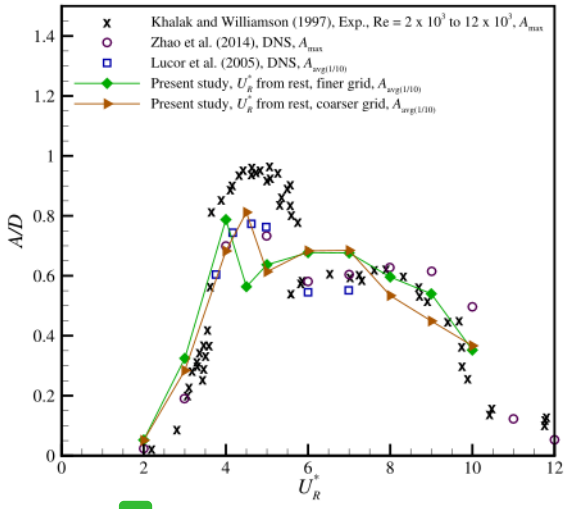

Fig. 10. $A_{avg(1/10)}$ vibration amplitudes over a range of reduced velocities at Re = 10^3 with the *rest* initial condition for the coarse and fine grids, compared with previously published studies.

amplitude of vibration is not a sufficient criterion to characterize the cylinder vibration because the maximum value may only occur once or twice, even over a long period of observation. Although the maximum value may be important in structural design to assess the maximum impact of vibrations, it does not convey enough information about the nature of oscillations. Moreover, if the energy generation potential of VIV of cylinders is to be investigated, the simple average of cylinder amplitudes (A_{avg}) is the most suitable characteristic. Due to a large number of previous studies only reporting A_{max} or $A_{avg(1/10)}$, perhaps all three or at least $A_{avg(1/10)}$ and A_{avg} both should be reported for future studies so that the vibrations can be characterized and compared with previous results, while also allowing for assessment of their energy generation potential.

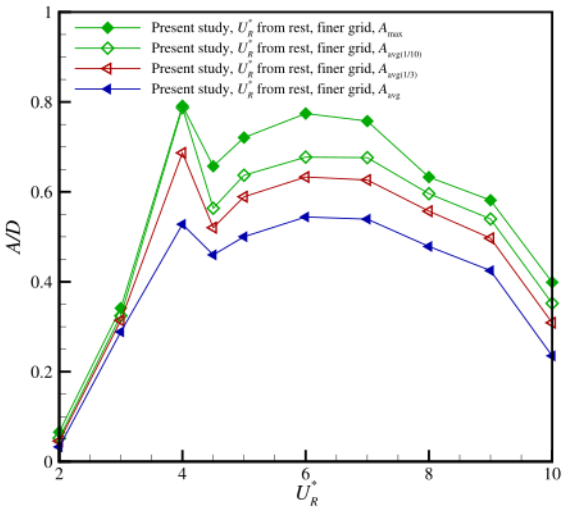

Fig. 11. Comparison of the different types of vibration amplitudes for a cylinder undergoing VIV at Re = 10^3 with the *rest* initial condition.

Fig. 12 shows the cylinder response frequency ratios for both the grids plotted against published studies. The cylinder response frequency ratio is the actual cylinder oscillation frequency normalized by the structural natural frequency in a vacuum. Although this frequency ratio is lower than earlier results shown in the figure, the earlier studies are either experimental or DNS studies. Previous LES studies of turbulent flow over a cylinder undergoing VIV have also been found to exhibit frequency ratios of less than one, such as Zhang and Dalton (1996) at Re = 13×10^3 and Al-Jamal and Dalton (2004) at Re = 8×10^3. This behaviour is known as soft-lock-in, where a slight detuning appears in the cylinder oscillation frequency. Mittal and Kumar (1999) concluded that the smaller mass ratio is the reason for this phenomenon. This conclusion is consistent with this present investigation, where the soft-lock-in does not appear in the laminar case with a larger mass ratio m^* = 149.1.

3.5. Further analysis of the turbulent regime under other initial conditions

Additional calculations were conducted for the same range of reduced velocities at Re = 10^3 with *increasing* U_R^* and *decreasing* U_R^* initial conditions. For each of the two types of studies, the cylinder was initially held stationary and then allowed to vibrate at the starting reduced velocity (U_R^* = 0.5 for the *increasing* U_R^* initial condition and U_R^* = 10.0 for the *decreasing* U_R^* initial condition). The reduced velocity was then varied with each step of ΔU^* = 0.5 after fixed simulation time intervals.

The results are shown in Figs. 13 and 14. The gradual overall increase in cylinder amplitudes can be observed through the initial branch of the lock-in region until the lower branch. Despite the average amplitudes showing a consistent variation through the lock-in region, significant fluctuations can be seen at most reduced velocities, which strengthens the argument for using either $A_{avg(1/10)}$ or A_{avg} for characterizing the amplitudes.

It is interesting to observe that in Fig. 13 for *increasing* U_R^* initial condition when U_R^* is increased from 4.0 to 4.5, the cylinder amplitude increases abruptly and displays a larger oscillation for a short duration before reducing to a smaller value. This leads to high values for A_{max} and $A_{avg(1/10)}$ amplitudes (shown in Figs. 15 and 16), even though A_{avg} would be much lower. Moreover, as discussed later, this short jump in amplitude is missing from the upper branch simulations for the *rest* and

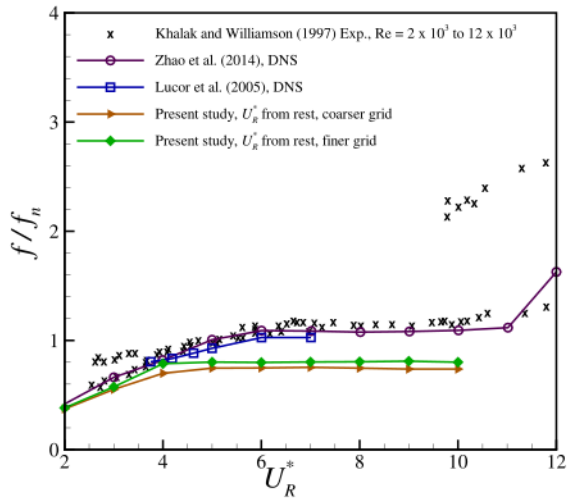

Fig. 12. Cylinder response frequency ratios over a range of reduced velocities at Re = 10^3 with the *rest* initial condition for the coarse and fine grids, compared with previously published studies.

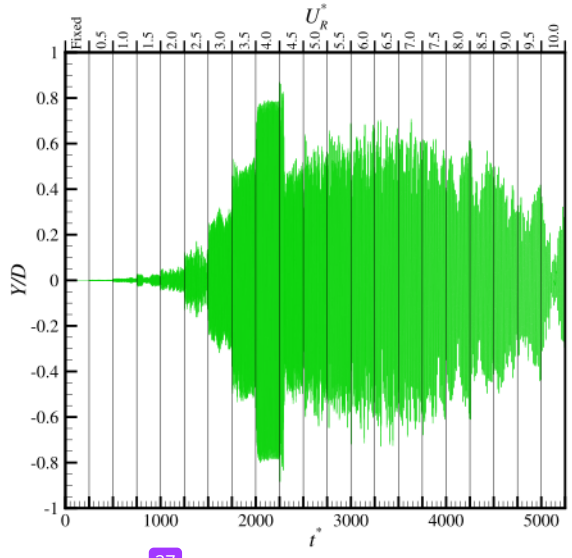

Fig. 13. Time history of a cylinder undergoing VIV at Re = 10^3 with the *increasing* U_R^* initial condition, and $\Delta U^* = 0.5$.

decreasing U_R^* initial conditions. Similarly, in Fig. 14 for *decreasing* U_R^* initial condition, when the U_R^* is changed from 4.0 to 3.5, a similar jump in cylinder amplitude occurs, which is not seen for the initial branch of the *rest* and *increasing* U_R^* initial conditions.

The A_{max} and $A_{avg(1/10)}$ amplitudes over the investigated reduced velocity range are plotted in Figs. 15 and 16, respectively. Although, $A_{avg(1/10)}$ for *increasing* U_R^* initial condition matches closely with the *rest* initial condition throughout the lock-in region, the A_{max} values for the *rest* initial condition are generally higher than those for *increasing* U_R^* initial condition in the upper branch. This suggests that a situation may occur when using the *rest* initial condition. On the other hand, a comparison between the *increasing* and *decreasing* U_R^* initial conditions reveals differences in the initial branch of the lock-in region as well as

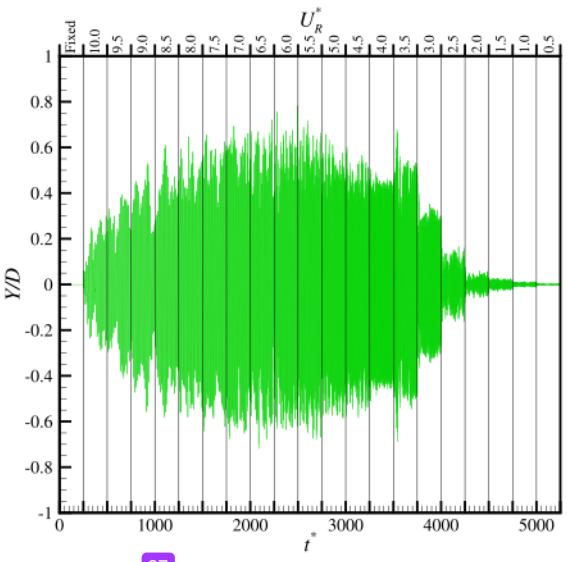

Fig. 14. Time history of a cylinder undergoing VIV at Re = 10^3 with the *decreasing* U_R^* initial condition, and $\Delta U^* = 0.5$.

in the upper branch. The initial branch amplitudes are slightly higher for the *decreasing* U_R^* initial condition, while the upper branch amplitudes are significantly higher for the *increasing* U_R^* initial condition. Therefore, a hysteresis phenomenon can be observed between the two types of initial conditions in turbulent flow cases, which is sketched in Fig. 17. In the present work, only a single blockage ratio of 5% has been used. However, Prasanth et al. (2006) investigated the effect of the blockage ratio for VIV in laminar flows and found that reducing the blockage from 5% to 1% caused the hysteresis in the initial branch to disappear, while the hysteresis in the lower branch persisted. Although their results are only applicable to low Reynolds numbers, the effect of the blockage ratio for the present case may also be investigated in the future to determine if it has any influence on this hysteresis phenomenon.

The cylinder response frequency ratios for the different types of initial conditions are represented in Fig. 18, which shows that the frequency ratios remain largely the same throughout the lock-in region.

To confirm the existence of the observed hysteresis phenomena and to rule out the presence of any numerical artefacts, the cases with increasing and decreasing initial conditions were re-run with the same parameters but with the change in reduced velocity, ΔU^*, at fixed simulation time intervals equal to 0.25. The time histories for the increasing and decreasing cases are given in Fig. 19.

The general trends are largely similar to the earlier case, with the hysteresis phenomenon distinguishable because the noticeably large vibrations at the onset of the lock-in regime in the *increasing* U_R^* initial condition case are absent from the *decreasing* U_R^* case. However, the smaller value of $\Delta U^* = 0.25$ leads to higher fluctuations of maximum amplitudes of vibration, especially during the lock-in region. A comparison of the A_{max} for the two ΔU^* cases reveals the greater fluctuations of vibration amplitudes for each of the initial conditions, as shown in Fig. 20.

Fig. 21 represents the instantaneous flow structures visualized using Q-criterion (Hunt et al., 1988) at a value of 0.01 for $U_R^* = 4.0$ and $= 4.25$, with both the increasing and decreasing initial conditions. The instantaneous vorticity contours for the same flow conditions are presented in Fig. 22. Since the fluctuations of the cylinder are larger for the *increasing* U_R^* initial condition, the flow is more chaotic with slightly

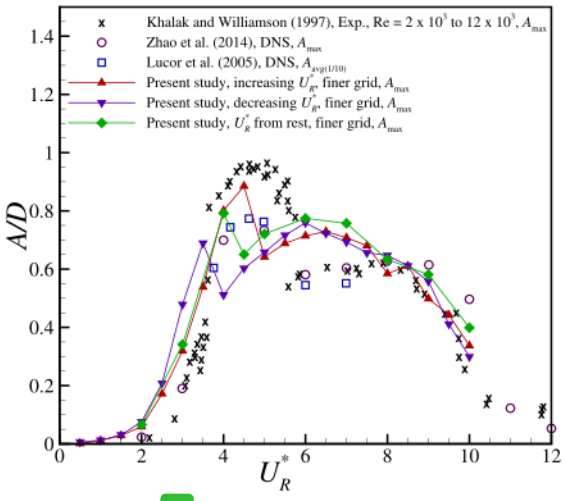

Fig. 15. Comparison of the maximum vibration amplitudes over a range of reduced velocities at Re = 10^3 for different initial conditions using the fine grid, compared with previously published studies.

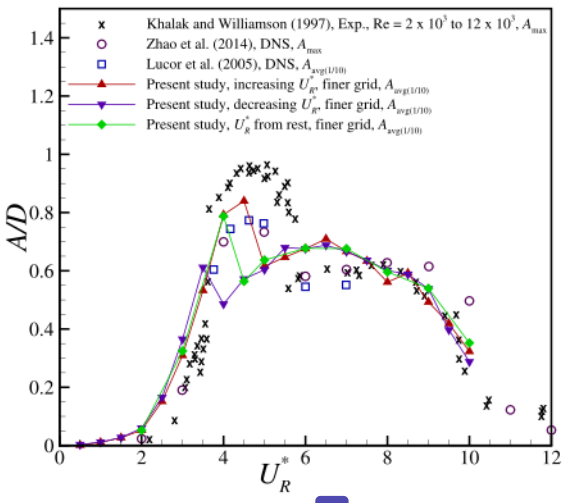

Fig. 16. Comparison of ($A_{avg(1/10)}$) amplitudes over a range of reduced velocities at Re = 10^3 for different initial conditions using the fine grid, compared with previously published studies.

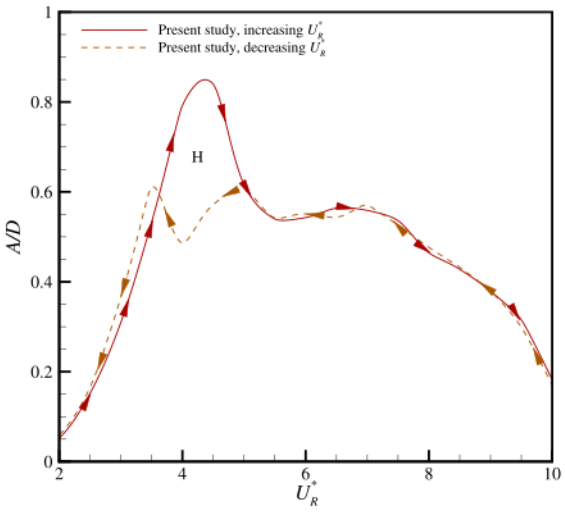

Fig. 17. Hysteresis phenomenon for a cylinder undergoing VIV at Re = 10^3 with *increasing* U_R^* and *decreasing* U_R^* initial conditions.

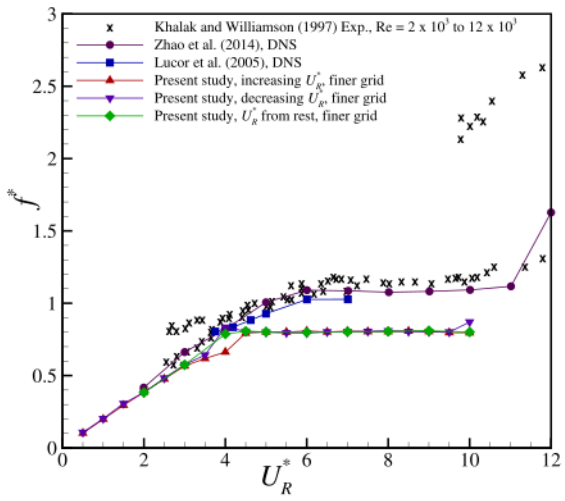

Fig. 18. Cylinder response frequency ratios over a range of reduced velocities at Re = 10^3 with different initial conditions, compared with previously published studies.

larger high vorticity structures. Otherwise, the nature of vortex-induced vibration is typical for flows in this regime and lock-in region. As shown in Fig. 22, two single vortices are formed behind the cylinder in every vibration cycle. This pattern is referred to the 2S mode vortex-shedding pattern (Govardhan and Williamson, 2000). Previous VIV simulation at Re = 1000 conducted by Zhao et al. (2014) also observed the same vortex-shedding pattern.

4. Conclusions

Flow over a circular cylinder undergoing vortex-induced vibration was investigated for laminar and turbulent regimes. The laminar flow cases were studied in the range of Re = 90–115 while the turbulent flow cases were conducted at Re = 10^3.

Multiple conventional grid independence tests were conducted for both sets of cases, and it was found that a single grid independence test was not sufficient to study VIV behaviour in the lock-in region, neither in laminar nor in turbulent flows. In both types of flows, there were two or more reduced velocities at which the coarse grid was able to match the values of the fine grid parameters sufficiently. However, detailed analyses revealed that at other reduced velocities, the fine grid led to more accurate results. For laminar flows, a coarser grid was also found to delay the onset of the lock-in region. Consequently, the importance of conducting multiple grid independence tests inside the lock-in region is established. For turbulent flows, it is preferable to conduct them at the beginning of the upper branch of the lock-in region.

An analysis of the time history of the laminar flow cases revealed that the grid refinement also affects the evolution of the vibration to a stable pattern with marked differences in the pattern for coarse and fine grids. Moreover, a stable vibration was achieved earlier for the

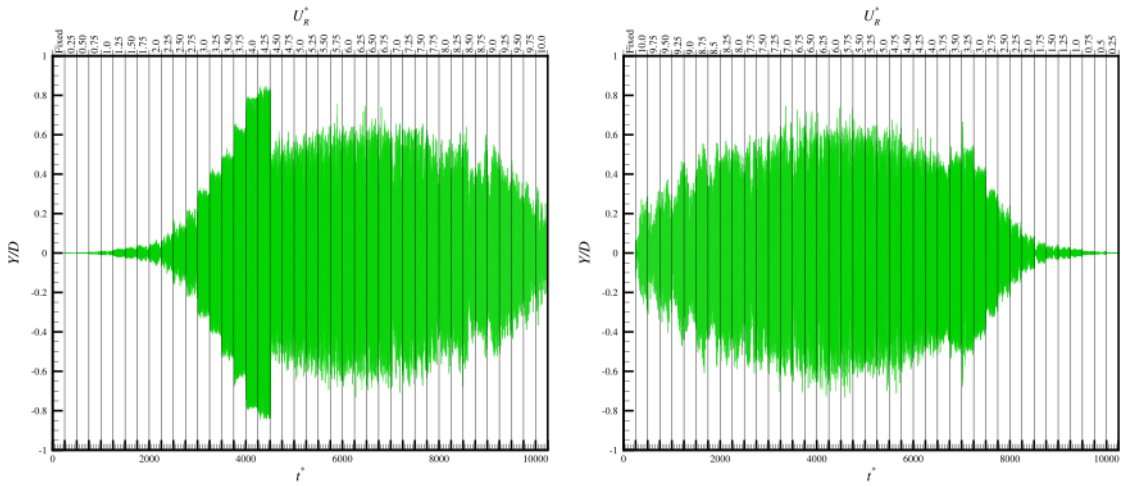

Fig. 19. Time histories of a cylinder undergoing VIV at Re = 10^3 with the *increasing* U_R^*(left) and decreasing U_R^*(right) initial conditions, and $\Delta U^* = 0.25$.

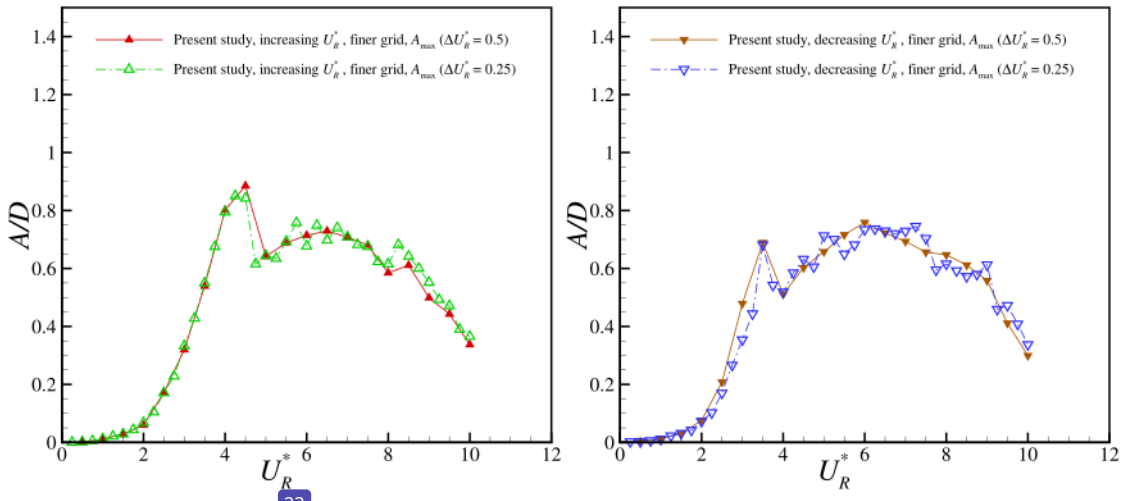

Fig. 20. Comparison of ($A_{avg(1/10)}$) amplitudes over a range of reduced velocities at Re = 10^3 for *increasing* U_R^*(left) and *decreasing* U_R^*(right) initial conditions with different ΔU^* values, compared with previously published studies.

finer grid in the upper branch of the lock-in region, while it took much longer in the lower branch as compared to the coarser grid.

On investigating the turbulent flows using different initial conditions, a hysteresis phenomenon was observed. The cases with the *increasing* U_R^* initial condition led to significantly higher amplitudes in the upper branch of the lock-in region, while the cases with the *decreasing* U_R^* initial condition exhibited lower amplitudes. However, in the initial branch, the *decreasing* U_R^* initial condition causes the cylinder to vibrate with slightly higher amplitudes than the other two initial conditions. The lower branch of the lock-in region is not affected by the changes in the initial conditions. The presence of hysteresis at a blockage ratio lower than 5% may be investigated in the future to determine its influence, if any.

Based on the investigations in this work, it was observed that A_{max} is not sufficient for a complete representation of the vibration characteristics of turbulent flow in the lock-in region. For future studies, the use of multiple calculation methods for vibration amplitudes is recommended such as $A_{avg(1/10)}$ and A_{avg}, as well as A_{max}.

Declaration of competing interest

The authors declare that they have no known competing financial interests or personal relationships that could have appeared to influence the work reported in this paper.

Data availability

Data will be made available on request.

Acknowledgements

The authors express their gratitude for the financial support from the Ministry of Science and Technology, Taiwan (grant no. MOST-110-2221-E-011-067) and thanks to the National Center for High-performance Computing (NCHC), Taiwan, for providing computational and storage resources.

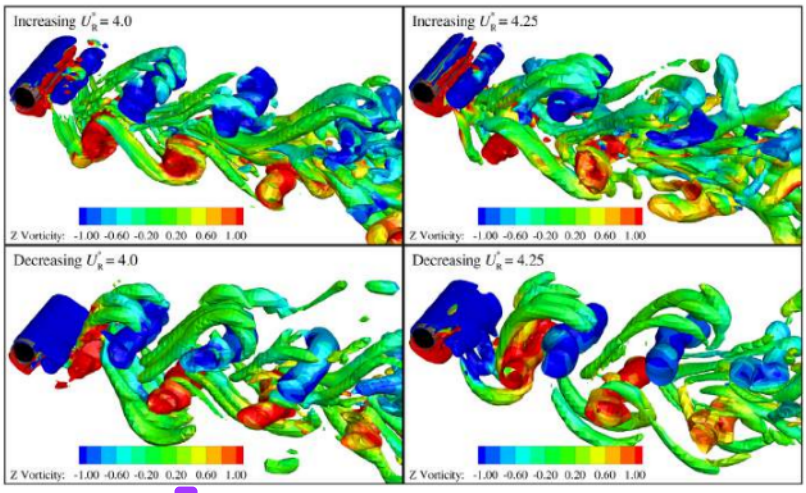

Fig. 21. Instantaneous flow structures visualized using Q-criterion at a value of 0.01 for $U_R^* = 4.0$ and $U_R^* = 4.25$, with both the *increasing* U_R^* and *decreasing* U_R^* initial conditions. The coloured contours represent the z-vorticity.

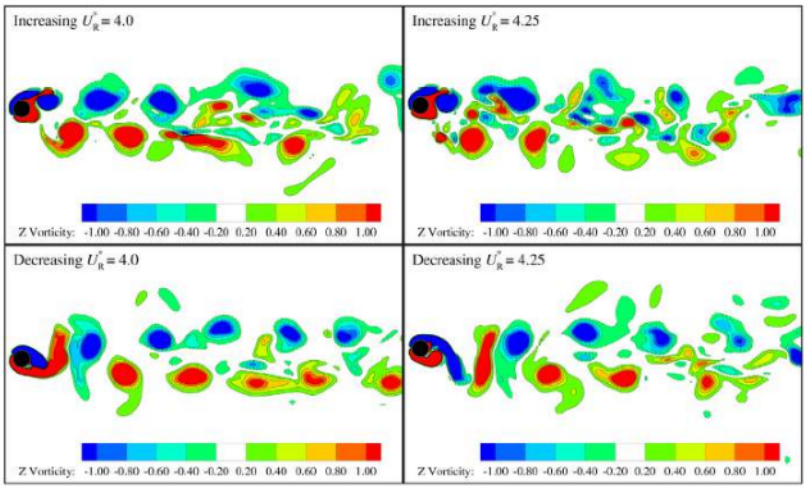

Fig. 22. The side-view of the instantaneous flow structures visualized using z-vorticity contours for $U_R^* = 4.0$ and $U_R^* = 4.25$, with both the *increasing* U_R^* and *decreasing* U_R^* initial conditions.

References

Al-Jamal, H., Dalton, C., 2004. Vortex induced vibrations using Large Eddy Simulation at a moderate Reynolds number. J. Fluids Struct. 19 (1), 73–92. http://dx.doi.org/10.1016/j.jfluidstructs.2003.10.005.

Anagnostopoulos, P., Bearman, P.W., 1992. Response characteristics of a vortex-excited cylinder at low Reynolds numbers. J. Fluids Struct. 6 (1), 39–50. http://dx.doi.org/10.1016/0889-9746(92)90054-7.

Bernitsas, M.M., Raghavan, K., Ben-Simon, Y., Garcia, E.M.H., 2008. VIVACE (vortex induced vibration aquatic clean energy): A New Concept in generation of clean and renewable energy from fluid flow. J. Offshore Mech. Arct. Eng. 130 (4), http://dx.doi.org/10.1115/1.2957913.

Chern, M.-J., Kuan, Y.-H., Nugroho, G., Lu, G.-T., Horng, T.-L., 2014. Direct-forcing immersed boundary modeling of vortex-induced vibration of a circular cylinder. J. Wind Eng. Ind. Aerodyn. 134, 109–121. http://dx.doi.org/10.1016/j.jweia.2014.08.015.

Chern, M.-J., Lu, G.T., Kuan, Y.H., Chakraborty, S., Nugroho, G., Liao, C.B., Horng, T.-L., 2018. Numerial study of vortex-induced vibration of circular cylinder adjacent to plane boundary using direct-forcing immersed boundary method. J. Mech. 34 (2), 177–191. http://dx.doi.org/10.1017/jmech.2017.55.

Chern, M.-J., Noor, D.Z., Liao, C.-B., Horng, T.-L., 2015. Direct-forcing immersed boundary method for mixed heat transfer. Commun. Comput. Phys. 18 (4), 1072–1094. http://dx.doi.org/10.4208/cicp.151214.250515s.

Dahl, J.M., Hover, F.S., Triantafyllou, M.S., Oakley, O.H., 2010. Dual resonance in vortex-induced vibrations at subcritical and supercritical Reynolds numbers. J. Fluid Mech. 643, 395–424. http://dx.doi.org/10.1017/S0022112009992060.

Dettmer, W., Perić, D., 2006. A computational framework for fluid–rigid body interaction: Finite element formulation and applications. In: A Tribute to Thomas J.R. Hughes on the Occasion of His 60th Birthday. Comput. Methods Appl. Mech. Engrg. 195 (13), 1633–1666. http://dx.doi.org/10.1016/j.cma.2005.05.033.

Ferguson, N., Parkinson, G.V., 1967. Surface and wake flow phenomena of the vortex-excited oscillation of a circular cylinder. J. Eng. Ind. 89 (4), 831–838. http://dx.doi.org/10.1115/1.3610163.

Govardhan, R., Williamson, C.H.K., 2000. Modes of vortex formation and frequency response of a freely vibrating cylinder. J. Fluid Mech. 420, 85–130. http://dx.doi.org/10.1017/S0022112000001233.

Gsell, S., Bourguet, R., Braza, M., 2016. Two-degree-of-freedom vortex-induced vibrations of a circular cylinder at Re=3900. J. Fluids Struct. 67, 156–172. http://dx.doi.org/10.1016/j.jfluidstructs.2016.09.004.

Guilmineau, E., Queutey, P., 2004. Numerical simulation of vortex-induced vibration of a circular cylinder with low mass-damping in a turbulent flow. J. Fluids Struct. 19 (4), 449–466. http://dx.doi.org/10.1016/j.jfluidstructs.2004.02.004.

Hover, F.S., Techet, A.H., Triantafyllou, M.S., 1998. Forces on oscillating uniform and tapered cylinders in a crossflow. J. Fluid Mech. 363, 97–114. http://dx.doi.org/10.1017/S0022112098001074.

Hunt, J.C.R., Wray, A.A., Moin, P., 1988. Eddies, streams, and convergence zones in turbulent flows. In: Studying Turbulence using Numerical Simulation Databases, 2. Proceedings of the 1988 Summer Program. Center for Turbulence Research, Stanford University, CA, United States, pp. 193–208, URL https://ui.adsabs.harvard.edu/abs/1988stun.proc..193H.

Khalak, A., Williamson, C.H.K., 1996. Dynamics of a hydroelastic cylinder with very low mass and damping. J. Fluids Struct. 10 (5), 455–472. http://dx.doi.org/10.1006/jfls.1996.0031.

Khalak, A., Williamson, C.H.K., 1997. Fluid forces and dynamics of a hydroelastic structure with very low mass and damping. J. Fluids Struct. 11 (8), 973–982. http://dx.doi.org/10.1006/jfls.1997.0110.

Khalak, A., Williamson, C.H.K., 1999. Motions, forces and mode transitions in vortex-induced vibrations at low mass-damping. J. Fluids Struct. 13 (7), 813–851. http://dx.doi.org/10.1006/jfls.1999.0236.

Labbé, D.F.L., Wilson, P.A., 2007. A numerical investigation of the effects of the spanwise length on the 3-D wake of a circular cylinder. J. Fluids Struct. 23 (8), 1168–1188. http://dx.doi.org/10.1016/j.jfluidstructs.2007.05.005.

Lei, C., Cheng, L., Kavanagh, K., 2001. Spanwise length effects on three-dimensional modelling of flow over a circular cylinder. Comput. Methods Appl. Mech. Engrg. 190 (22), 2909–2923. http://dx.doi.org/10.1016/S0045-7825(00)00272-3.

Leonard, B.P., 1979. A stable and accurate convective modelling procedure based on quadratic upstream interpolation. Comput. Methods Appl. Mech. Engrg. 19 (1), 59–98. http://dx.doi.org/10.1016/0045-7825(79)90034-3.

Liu, B., Jaiman, R.K., 2018. Dynamics and stability of gap-flow interference in a vibrating side-by-side arrangement of two circular cylinders. J. Fluid Mech. 855, 804–838. http://dx.doi.org/10.1017/jfm.2018.651.

Lucor, D., Foo, J., Karniadakis, G.E., 2005. Vortex mode selection of a rigid cylinder subject to VIV at low mass-damping. In: Bluff-Body/Flow Interactions. J. Fluids Struct. 20 (4), 483–503. http://dx.doi.org/10.1016/j.jfluidstructs.2005.02.002.

Mittal, S., Kumar, V., 1999. Finite element study of vortex-induced cross-flow and in-line oscillations of a circular cylinder at low reynolds numbers. Internat. J. Numer. Methods Fluids 31 (7), 1087–1120. http://dx.doi.org/10.1002/(SICI)1097-0363(19991215)31:7<1087::AID-FLD911>3.0.CO;2-C.

Navrose, Mittal, S., 2013. Free vibrations of a cylinder: 3-d computations at re=1000. In: Special Issue on Bluff Body Flows (Blubof2011). J. Fluids Struct. 41, 109–118. http://dx.doi.org/10.1016/j.jfluidstructs.2013.02.017.

NCHC, 2021. National center for high-performance computing, Taiwan. URL https://www.nchc.org.tw.

Pan, Z.Y., Cui, W.C., Miao, Q.M., 2007. Numerical simulation of vortex-induced vibration of a circular cylinder at low mass-damping using RANS code. J. Fluids Struct. 23 (1), 23–37. http://dx.doi.org/10.1016/j.jfluidstructs.2006.07.007.

Pastrana, D., Cajas, J.C., Lehmkuhl, O., Rodríguez, I., Houzeaux, G., 2018. Large-eddy simulations of the vortex-induced vibration of a low mass ratio two-degree-of-freedom circular cylinder at subcritical Reynolds numbers. Comput. & Fluids 173, 118–132. http://dx.doi.org/10.1016/j.compfluid.2018.03.016.

Prasanth, T.K., Behara, S., Singh, S.P., Kumar, R., Mittal, S., 2006. Effect of blockage on vortex-induced vibrations at low Reynolds numbers. In: "Bluff Body Wakes and Vortex-Induced Vibrations (BBVIV-4). J. Fluids Struct. 22 (6), 865–876. http://dx.doi.org/10.1016/j.jfluidstructs.2006.04.011.

Prasanth, T.K., Premchandran, V., Mittal, S., 2011. Hysteresis in vortex-induced vibrations: critical blockage and effect of m*. J. Fluid Mech. 671, 207–225. http://dx.doi.org/10.1017/S0022112010005537, Publisher: Cambridge University Press.

Raza, S.A., Chern, M.-J., Susanto, H., Zhou, Y.-H., 2020. Numerical investigation of the effects of a small fixed sphere in tandem arrangement on VIV of a sphere. J. Wind Eng. Ind. Aerodyn. 206, 104368. http://dx.doi.org/10.1016/j.jweia.2020.104368.

Raza, S.A., Irawan, Y.H., Chern, M.-J., 2021. Effect of boundary conditions and domain size on the turbulent flow characteristics over a circular cylinder. J. Chin. Inst. Eng. 44 (7), 659–672. http://dx.doi.org/10.1080/02533839.2021.1940295.

Roshko, A., 1953. On the development of turbulent wakes from vortex streets. Report or Paper, National Advisory Committee for Aeronautics, Washington, DC, p. 80, URL https://resolver.caltech.edu/CaltechAUTHORS:20141114-105935749.

Roshko, A., 1954. On the development of turbulent wakes from vortex streets. Report or Paper, National Advisory Committee for Aeronautics, Washington, D. C., p. 27, URL https://resolver.caltech.edu/CaltechAUTHORS:ROSnacarpt1191.

Sarpkaya, T., 2004. A critical review of the intrinsic nature of vortex-induced vibrations. J. Fluids Struct. 19 (4), 389–447. http://dx.doi.org/10.1016/j.jfluidstructs.2004.02.005.

Sidebottom, W., Ooi, A., Jones, D., 2015. A parametric study of turbulent flow past a circular cylinder using large eddy simulation. J. Fluids Eng. 137 (9), http://dx.doi.org/10.1115/1.4030380.

Smagorinsky, J., 1963. General circulation experiments with the primitive equations. Mon. Weather Rev. 91 (3), 99–164. http://dx.doi.org/10.1175/1520-0493(1963)091<0099:GCEWTP>2.3.CO;2.

Sun, X., Dalton, C., 1994. Application of two SGS models to flow past a circular cylinder. In: Proceedings of the 1994 International Mechanical Engineering Congress and Exposition. 203, ASME, New York, NY, United States, Chicago, IL, USA, pp. 21–29.

Wang, E., Xiao, Q., Incecik, A., 2017. Three-dimensional numerical simulation of two-degree-of-freedom VIV of a circular cylinder with varying natural frequency ratios at Re=500. J. Fluids Struct. 73, 162–182. http://dx.doi.org/10.1016/j.jfluidstructs.2017.06.001.

Yang, J., Preidikman, S., Balaras, E., 2008. A strongly coupled, embedded-boundary method for fluid–structure interactions of elastically mounted rigid bodies. J. Fluids Struct. 24 (2), 167–182. http://dx.doi.org/10.1016/j.jfluidstructs.2007.08.002.

Zhang, J., Dalton, C., 1996. Interactions of vortex-induced vibrations of a circular cylinder and a steady approach flow at a Reynolds number of 13,000. Comput. & Fluids 25 (3), 283–294. http://dx.doi.org/10.1016/0045-7930(95)00040-2.

Zhao, M., Cheng, L., An, H., Lu, L., 2014. Three-dimensional numerical simulation of vortex-induced vibration of an elastically mounted rigid circular cylinder in steady current. J. Fluids Struct. 50, 292–311. http://dx.doi.org/10.1016/j.jfluidstructs.2014.05.016.

Effect of grid size and initial conditions on vortex-induced vibration of a circular cylinder

ORIGINALITY REPORT

22%	15%	20%	3%
SIMILARITY INDEX	INTERNET SOURCES	PUBLICATIONS	STUDENT PAPERS

PRIMARY SOURCES

1	repository.ubaya.ac.id Internet Source	1%
2	Yosua Heru Irawan, Syed Ahmad Raza, Ming-Jyh Chern. "Passively enhanced VIV responses of side-by-side cylinders at moderate Reynolds number", Applied Ocean Research, 2023 Publication	1%
3	Desta Goytom Tewolde, Zi-Hsuan Wei, Ming-Jyh Chern. "Numerical modeling of flow past a volumeless and thin rigid body using direct forcing immersed boundary method", International Journal for Numerical Methods in Fluids, 2022 Publication	1%
4	doi.org Internet Source	1%
5	newton.math.fcu.edu.tw Internet Source	1%

6	Yosua Heru Irawan, Yu-Hao Chiu, Syed Ahmad Raza, Ming-Jyh Chern. "Influence of upstream staggered cylinder on vortex-induced vibration responses of side-by-side cylinders in turbulent flow", Physics of Fluids, 2023 Publication	1 %
7	Navrose, Sanjay Mittal. "Vibrations of a cylinder in a uniform flow in the presence of a no-slip side-wall", Journal of Fluids and Structures, 2015 Publication	1 %
8	cris.unibo.it Internet Source	1 %
9	aip.scitation.org Internet Source	1 %
10	researchdirect.westernsydney.edu.au Internet Source	<1 %
11	www.cambridge.org Internet Source	<1 %
12	link.springer.com Internet Source	<1 %
13	oatao.univ-toulouse.fr Internet Source	<1 %
14	Ming-Jyh Chern, Chin-Cheng Wang, Zi-Hsuan Wei, Ping-Chien Lu. "Numerical Investigation	<1 %

of a Pitching NACA 0012 Wing with Plasma-Based Flow Control Using Prediction–Correction Direct-Forcing Immersed Boundary Method", Journal of Aerospace Engineering, 2023
Publication

15	Submitted to City University of Hong Kong Student Paper	<1 %
16	Pan, Z.Y.. "Numerical simulation of vortex-induced vibration of a circular cylinder at low mass-damping using RANS code", Journal of Fluids and Structures, 200701 Publication	<1 %
17	Yan Bao, Cheng Huang, Dai Zhou, Jiahuang Tu, Zhaolong Han. "Two-degree-of-freedom flow-induced vibrations on isolated and tandem cylinders with varying natural frequency ratios", Journal of Fluids and Structures, 2012 Publication	<1 %
18	espace.curtin.edu.au Internet Source	<1 %
19	research-repository.griffith.edu.au Internet Source	<1 %
20	www.escholar.manchester.ac.uk Internet Source	<1 %

flair.monash.edu

21	Internet Source	<1%
22	ntnuopen.ntnu.no Internet Source	<1%
23	Seyedmohammad Mousavisani, Naumi Noshin Chowdhury, Hadi Samsam-Khayani, Hamed Samandari, Banafsheh Seyed-Aghazadeh. "Vortex-induced vibration of a two degree-of-freedom flexibly mounted circular cylinder in the crossflow direction", Journal of Fluid Mechanics, 2022 Publication	<1%
24	flair.monash.edu.au Internet Source	<1%
25	windeng.t.u-tokyo.ac.jp Internet Source	<1%
26	W. Dettmer, D. Perić. "A computational framework for fluid–rigid body interaction: Finite element formulation and applications", Computer Methods in Applied Mechanics and Engineering, 2006 Publication	<1%
27	Ying Wu, Zhi Cheng, Ryley McConkey, Fue-Sang Lien, Eugene Yee. "Modelling of Flow-Induced Vibration of Bluff Bodies: A Comprehensive Survey and Future Prospects", Energies, 2022	<1%

	Publication	
28	openaccess.city.ac.uk Internet Source	<1 %
29	Seyyed M. Hasheminejad, Milad Naderi, Yasin Masoumi. "Cross-flow VIV mitigation of a near-bottom underwater pipeline using rigid and flexible smart wall-mounted control plates", Ocean Engineering, 2024 Publication	<1 %
30	Submitted to Tarleton State University Student Paper	<1 %
31	c.coek.info Internet Source	<1 %
32	shellbuckling.com Internet Source	<1 %
33	deepblue.lib.umich.edu Internet Source	<1 %
34	Prasanth, T.K.. "Effect of blockage on vortex-induced vibrations at low Reynolds numbers", Journal of Fluids and Structures, 200608/10 Publication	<1 %
35	dokumen.pub Internet Source	<1 %
36	par.nsf.gov Internet Source	<1 %

37	Submitted to Indian Institute of Technology, Madras Student Paper	<1%
38	J. Shao, C. Zhang. "Large eddy simulations of the flow past two side-by-side circular cylinders", International Journal of Computational Fluid Dynamics, 2008 Publication	<1%
39	www.semanticscholar.org Internet Source	<1%
40	Athanasios E. Giannenas, Nikolaos Bempedelis, Felipe N. Schuch, Sylvain Laizet. "A Cartesian Immersed Boundary Method Based on 1D Flow Reconstructions for High-Fidelity Simulations of Incompressible Turbulent Flows Around Moving Objects", Flow, Turbulence and Combustion, 2022 Publication	<1%
41	Singh, S.P.. "Vortex-induced oscillations at low Reynolds numbers: Hysteresis and vortex-shedding modes", Journal of Fluids and Structures, 200511 Publication	<1%
42	Computational Fluid Dynamics 2000, 2001. Publication	<1%
43	Fotini Katopodes Chow, Robert L. Street, Ming Xue, Joel H. Ferziger. "Explicit Filtering and	<1%

Reconstruction Turbulence Modeling for Large-Eddy Simulation of Neutral Boundary Layer Flow", Journal of the Atmospheric Sciences, 2005
Publication

---

44 Wei Chen, Chang-Kyu Rheem, Yuanzhou Zheng, Atilla Incecik, Yongshui Lin, Zhixiong Li. "Discrete-vortex analysis of high Reynolds number flow past a rotating cylinder", AIP Advances, 2020 <1%
Publication

---

45 Xiangxi Han, Youhong Tang, Zhanbin Meng, Fei Fu, Ang Qiu, Jian Gu, Jiaming Wu. "Surface roughness effect on cylinder vortex-induced vibration at moderate Re regimes", Ocean Engineering, 2021 <1%
Publication

---

46 www.hindawi.com <1%
Internet Source

---

47 MITTAL, S.. "CONTROL OF FLOW PAST BLUFF BODIES USING ROTATING CONTROL CYLINDERS", Journal of Fluids and Structures, 200102 <1%
Publication

---

48 Submitted to National Chin-Yi University of Technology <1%
Student Paper

49	en.wikipedia.org Internet Source	<1 %
50	eprints.gla.ac.uk Internet Source	<1 %
51	midra.uni-miskolc.hu Internet Source	<1 %
52	pubs.aip.org Internet Source	<1 %
53	Banafsheh Seyed-Aghazadeh, Daniel W. Carlson, Yahya Modarres-Sadeghi. "Vortex-induced vibration and galloping of prisms with triangular cross-sections", Journal of Fluid Mechanics, 2017 Publication	<1 %
54	Fan Yang, Zhongbing Zhou, Xiaofan Lou, Lin Lu. "Flow around a near-bed horizontal circular cylinder mounted on a vertical wall", Ocean Engineering, 2020 Publication	<1 %
55	Hemanshul Garg, Atul Kumar Soti, Rajneesh Bhardwaj. "Vortex-induced vibration and galloping of a circular cylinder in presence of cross-flow thermal buoyancy", Physics of Fluids, 2019 Publication	<1 %

56	M. H. Bahmani, M. H. Akbari. "Response characteristics of a vortex-excited circular cylinder in laminar flow", Journal of Mechanical Science and Technology, 2011 Publication	<1 %
57	Mia Abrahamsen Prsic, Muk Chen Ong, Bjørnar Pettersen, Dag Myrhaug. "Large Eddy Simulations of flow around a smooth circular cylinder in a uniform current in the subcritical flow regime", Ocean Engineering, 2014 Publication	<1 %
58	Mohammad Athar Khan, Saif Masood, Md. Abu Shahzer, Syed Fahad Anwar. "Augmentation of VIVACE by means of Thermal Buoyancy", IOP Conference Series: Materials Science and Engineering, 2020 Publication	<1 %
59	Subhankar Sen. "Wake modes of a freely vibrating square cylinder", Physics of Fluids, 2022 Publication	<1 %
60	eprints.ncl.ac.uk Internet Source	<1 %
61	fedetd.mis.nsysu.edu.tw Internet Source	<1 %
62	stax.strath.ac.uk Internet Source	<1 %

63	Al Jamal, H.. "The contrast in phase angles between forced and self-excited oscillations of a circular cylinder", Journal of Fluids and Structures, 200505 Publication	<1 %
64	M. S. Day. "Numerical simulation of laminar reacting flows with complex chemistry", Combustion Theory and Modelling, 12/1/2000 Publication	<1 %
65	Marek Jan Janocha, Muk Chen Ong, Guang Yin. "Large eddy simulations and modal decomposition analysis of flow past a cylinder subject to flow-induced vibration", Physics of Fluids, 2022 Publication	<1 %
66	Ming Zhao, Liang Cheng, Hongwei An, Lin Lu. "Three-dimensional numerical simulation of vortex-induced vibration of an elastically mounted rigid circular cylinder in steady current", Journal of Fluids and Structures, 2014 Publication	<1 %
67	Zhao, M.. "Direct numerical simulation of three-dimensional flow past a yawed circular cylinder of infinite length", Journal of Fluids and Structures, 200907 Publication	<1 %

68	Zhendong Cui, Ming Zhao, Bin Teng, Liang Cheng. "Two-dimensional numerical study of vortex-induced vibration and galloping of square and rectangular cylinders in steady flow", Ocean Engineering, 2015 Publication	<1 %
69	Zhong Li, Weigang Yao, Rajeev K. Jaiman, Boo Cheong Khoo. "On the Streamwise Oscillations of Freely Vibrating Cylinder Near a Stationary Plane Wall in Steady Flow", Volume 2: CFD and VIV, 2016 Publication	<1 %
70	ascelibrary.org Internet Source	<1 %
71	cpb-us-w2.wpmucdn.com Internet Source	<1 %
72	rms.scu.ac.ir Internet Source	<1 %
73	www.mdpi.com Internet Source	<1 %
74	"Proceedings of the International Conference on Modern Research in Aerospace Engineering", Springer Science and Business Media LLC, 2018 Publication	<1 %
75	9512.net Internet Source	

<1%

76 Cheol-Min Lee, Kwang-Jun Paik, Eun Soo Kim, Inwon Lee. "A fluid–structure interaction simulation on the wake-induced vibration of tandem cylinders with pivoted rotational motion", Physics of Fluids, 2021 <1%
Publication

77 D. Pastrana, I. Rodriguez, J.C. Cajas, O. Lehmkuhl, G. Houzeaux. "On the formation of Taylor-Görtler structures in the vortex induced vibration phenomenon", International Journal of Heat and Fluid Flow, 2020 <1%
Publication

78 D. Pastrana, J.C. Cajas, O. Lehmkuhl, I. Rodríguez, G. Houzeaux. "Large-eddy simulations of the vortex-induced vibration of a low mass ratio two-degree-of-freedom circular cylinder at subcritical Reynolds numbers", Computers & Fluids, 2018 <1%
Publication

79 E. Konstantinidis, J. Zhao, J. Leontini, D. Lo Jacono, J. Sheridan. "Phase dynamics of effective drag and lift components in vortex-induced vibration at low mass–damping", Journal of Fluids and Structures, 2020 <1%
Publication

80	Francisco J. Huera-Huarte. "Dynamics and excitation in a low mass-dampingcylinder in cross-flow withside-by-side interference", Journal of Fluid Mechanics, 2018 Publication	<1 %
81	Lixia Qu, Christoffer Norberg, Lars Davidson, Shia-Hui Peng, Fujun Wang. "Quantitative numerical analysis of flow past a circular cylinder at Reynolds number between 50 and 200", Journal of Fluids and Structures, 2013 Publication	<1 %
82	M.S. Chislett. "Marine Simulation and Ship Manoeuvrability", CRC Press, 2021 Publication	<1 %
83	Ping Chun Wu, Yin-Hung Lin, Lei Fang Tsai, Ming Hung Chen, Pei-Lung Chen, Shun-Chung Pai. "ABO genotyping with next-generation sequencing to resolve heterogeneity in donors with serology discrepancies", Transfusion, 2018 Publication	<1 %
84	Ruilin Zhang, Zhiwen Liu, Lianhua Wang, Zhengqing Chen. "Component decomposition and spatial distribution of unsteady forces on a circular cylinder oscillated under various amplitudes at Re = 2.0×104", Ocean Engineering, 2023 Publication	<1 %

85	W. Sidebottom, A. Ooi, D. Jones. "A Parametric Study of Turbulent Flow Past a Circular Cylinder Using Large Eddy Simulation", Journal of Fluids Engineering, 2015 Publication	<1 %
86	Wolfgang Balzer, Hermann Fasel. "Direct Numerical Simulation of Laminar Boundary-Layer Separation and Separation Control on the Suction Side of an Airfoil at Low Reynolds Number Conditions", 40th Fluid Dynamics Conference and Exhibit, 2010 Publication	<1 %
87	Wu, X.. "A review of recent studies on vortex-induced vibrations of long slender cylinders", Journal of Fluids and Structures, 201201 Publication	<1 %
88	curve.coventry.ac.uk Internet Source	<1 %
89	hal.archives-ouvertes.fr Internet Source	<1 %
90	psecommunity.org Internet Source	<1 %
91	real.mtak.hu Internet Source	<1 %
92	repositorio2.unican.es Internet Source	<1 %

93	Bowen Ma, Narakorn Srinil. "Two-dimensional vortex-induced vibration suppression through the cylinder transverse linear/nonlinear velocity feedback", Acta Mechanica, 2017 Publication	<1 %
94	IUTAM Bookseries, 2009. Publication	<1 %
95	Sadik Kakaç, Yaman Yener, Anchasa Pramuanjaroenkij. "Convective Heat Transfer", CRC Press, 2013 Publication	<1 %
96	Bhattacharjee, P.. "Simulations of laminar and transitional cold wall jets", International Journal of Heat and Fluid Flow, 200402 Publication	<1 %
97	Chung, Meng-Hsuan. "Transverse vortex-induced vibration of spring-supported circular cylinder translating near a plane wall", European Journal of Mechanics - B/Fluids, 2016. Publication	<1 %
98	Enhao Wang, Wanhai Xu, Xifeng Gao, Liqin Liu, Qing Xiao, Kiran Ramesh. "The effect of cubic stiffness nonlinearity on the vortex-induced vibration of a circular cylinder at low Reynolds numbers", Ocean Engineering, 2019 Publication	<1 %

99	George C. Christodoulou, Anastasios I. Stamou. "Environmental Hydraulics", CRC Press, 2010 Publication	<1 %
100	Mehmood, Arshad, Muhammad R. Hajj, Ali Nayfeh, and Abdullah Nuhait. "Effectiveness of Nonlinear Energy Sink (NES) in Suppressing Vortex-Induced Vibrations of a Circular Cylinder", 54th AIAA/ASME/ASCE/AHS/ASC Structures Structural Dynamics and Materials Conference, 2013. Publication	<1 %
101	Reza Maryami, Elias J.G. Arcondoulis, Yu Liu. "Flow and aerodynamic noise control of a circular cylinder by local blowing", Journal of Fluid Mechanics, 2024 Publication	<1 %
102	Tian Li, Takeshi Ishihara. "Numerical study on vortex-induced vibration of circular cylinder with two-degree-of-freedom and geometrical nonlinear system", Journal of Fluids and Structures, 2021 Publication	<1 %
103	Wanhai Xu, Haokai Wu, Kun Jia, Enhao Wang. "Numerical investigation into the effect of spacing on the flow-induced vibrations of two tandem circular cylinders at subcritical Reynolds numbers", Ocean Engineering, 2021	<1 %

Publication

104	Zhuang Kang, Caihong Yang, Cheng Zhang, Rui Chang, Yunhe Zhai. "Modification and application of low Reynolds number k–ε turbulence model to vortex-induced vibration at subcritical Reynolds number range", Journal of Marine Science and Technology, 2020 Publication	<1 %
105	Lucor, D.. "Vortex mode selection of a rigid cylinder subject to VIV at low mass-damping", Journal of Fluids and Structures, 200505 Publication	<1 %

Exclude quotes	On	Exclude matches	Off
Exclude bibliography	On		